analytical chemistry

Technical Note

Cite This: *Anal. Chem.* 2018, 90, 5563−5568

pubs.acs.org/ac

An Affordable and Portable Thermocycler for Real-Time PCR Made of 3D-Printed Parts and Off-the-Shelf Electronics

Roberto A. Mendoza-Gallegos, Amelia Rios, and Jose L. Garcia-Cordero*

Unidad Monterrey, Centro de Investigación y de Estudios Avanzados del Instituto Politécnico Nacional, Parque PIIT, Apodaca, Nuevo León C.P. 66628, Mexico

Supporting Information

ABSTRACT: The polymerase chain reaction (PCR) is a sought-after nucleic acid amplification technique used in the detection of several diseases. However, one of the main limitations of this and other nucleic acid amplification assays is the complexity, size, maintenance, and cost of their operational instrumentation. This limits the use of PCR applications in settings that cannot afford the instruments but that may have access to basic electrical, electronic, and optical components and the expertise to build them. To provide a more accessible platform, we developed a low-cost, palm-size, and portable instrument to perform real-time PCR (qPCR). The thermocycler leverages a copper-sheathed power resistor and a computer fan, in tandem with basic electronic components controlled from a single-board computer. The instrument incorporates a 3D-printed chassis and a custom-made fluorescence optical setup based on a CMOS camera and a blue LED. Results are displayed in real-time on a tablet. We also fabricated simple acrylic microdevices consisting of four wells (2 μL in volume each) where PCR reactions take place. To test our instrument, we performed qPCR on a series of cDNA dilutions spanning 4 orders of magnitude, achieving similar limits of detection as those achieved by a benchtop thermocycler. We envision our instrument being utilized to enable routine monitoring and diagnosis of certain diseases in low-resource areas.

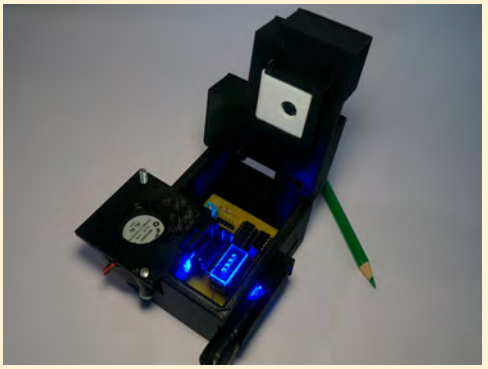

The polymerase chain reaction (PCR), a nucleic acid amplification (NAA) assay, is a very powerful and sensitive method used to quantify DNA and mRNA expression for clinical diagnosis.[1,2] PCR is the method of choice recommended by the World Health Organization (WHO) to detect some viral epidemics like Ebola[3] and Zika.[4] It is also the most popular and robust method for pathogen detection.[5,6] PCR was the first technique to amplify nucleic acids, and its popularity is due to the large dynamic range (6−7 orders of magnitude) and the high detection sensitivity and specificity that it achieves.[7] Furthermore, there are public databases, such as PrimerBank, that contain validated primer sequences for most human genes. In addition, PCR also encompasses a variety of applications including forensics, paternity tests, food and water safety, genetic disorders, cancer, mutation studies, among others.[8−11]

Nevertheless, a common misconception surrounding PCR applications is that because they require complex thermal management,[2] the design and construction of its operational instrumentation inevitably becomes bulky, heavy (∼9 kg), power-hungry (hundreds of watts of consumption), and expensive: characteristics that make them available predominately to centralized laboratories in developed countries.[2,4,8,9,12−16] Similar arguments can be made for developing real-time PCR (qPCR) instrumentation (which makes it faster, simpler, and more quantitative than regular PCR[12,15]) but that nonetheless requires a complex and expensive optical setup[16] to measure fluorescent signals from amplicons at the end of each cycle.

The high cost of instruments for real-time PCR, in addition to their high maintenance cost, has prevented their adoption in less-developed countries with limited laboratory infrastructure,[9,12,14,15] particularly in rural zones of the developing world, which are generally under-resourced and where disease outbreaks are more likely to occur.[12] Therefore, access to low-cost instrumentation could enable faster diagnosis and routine monitoring of certain diseases.[9,17] For example, despite an urgent need, the WHO does not recommend the use of viral load testing in resource-limited countries due to a lack of laboratory facilities and instrumentation, and as a result such testing is not routinely performed.[17]

It is apparent that the development of small, portable, and inexpensive real-time PCR instruments is critical for global health.[8,16,18] Ideally, such an instrument would be made of modular and low-weight parts allowing for quick assembly and low-cost shipping. In addition, it should be constructed with readily available consumer electronics for quick assembly and repairs as needed. It must be robust with the ability to operate within a wide range of temperatures, and it should be powered

Received: November 22, 2017
Accepted: April 6, 2018
Published: April 6, 2018

DOI: 10.1021/acs.analchem.7b04843
Anal. Chem. 2018, 90, 5563−5568

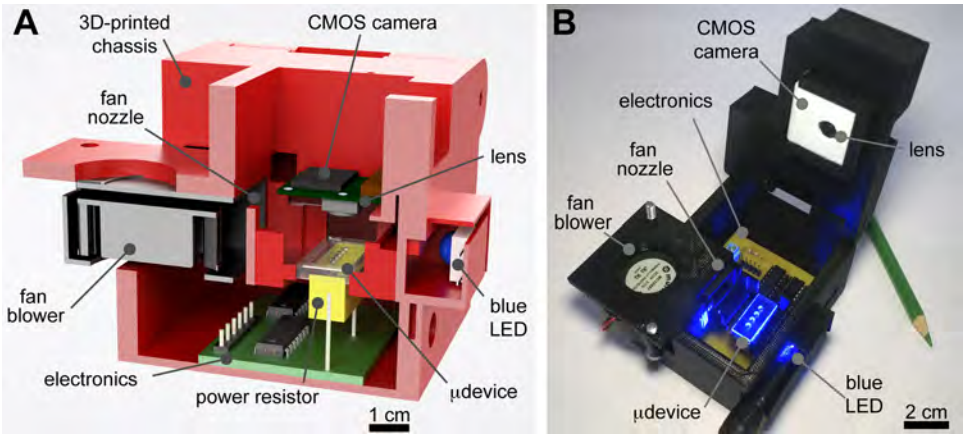

Figure 1. (A) 3D render of a cross-sectional view of the RT-PCR instrument showing its different components. (B) Photograph of the actual instrument with the lid open. Illumination from the blue LED can be seen.

by a battery or have low-energy consumption, to allow for operation in areas with limited access to a reliable energy source. Finally, it should rely on open-source platforms such that the software can be easily programmed, fixed, redistributed, and updated as required. These characteristics could enable electrical/electronic technicians or engineering students in the developing world to build such an instrument in a basic workshop.

Since the first demonstrations of portable PCR instrumentation,[19−24] several research groups have demonstrated significant progress in some of these aspirational characteristics.[1,3,5,7,8,10,12−14,16,25−32] However, there are still unfulfilled gaps concerning the development of a thorough and integrated instrument with all or most of these ideal characteristics. In an effort to tackle most of these issues, we present a design for an affordable thermocycler with an integrated fluorescent module for quantitative PCR. This instrument is made of 3D-printed parts and easily accessible, off-the-shelf electronics. Thermal cycling is enabled by two inexpensive consumer electronics parts: a power resistor and a computer fan. The electronics and tablet, where results are displayed in real-time, are controlled from a single-board computer. We also developed devices consisting of four microwells made of acrylic via rapid prototyping. We characterized our instrument by carrying out qPCR reactions and found similar limits of detections compared to those of a commercial benchtop thermocycler.

MATERIALS AND METHODS

Thermocycler. The core of the thermocycler is a 50 Ω, 5 W cement power resistor (280CR5−50-RC, Mouser, U.S.A.) and a computer fan blower (71P8674, Newark Element14). The fan nozzle was faced directly onto the resistor. To homogenize the temperature on the resistor surface, we wrapped it with conductive copper tape (T118112, 3M) and commercial aluminum foil. The temperature was monitored in real-time with a NTC thermistor (B57540G0502 + 002, Epcos) connected to an analog-to-digital converter (ADC, MCP3008, Microchip). The heater and the blower are controlled with an algorithm that uses pulse width modulation (PWM) integrated into a proportional integration derivative (PID) control. See Figure S-1 for the circuit schematic and Figure S-2 for a photograph of the PCB. Additional information can be found in the Supporting Information. The instrument is powered by a 24 V power supply (VCS50US24, XP Power).

3D Printing Chassis. The 3D parts for the instrument were designed in Inventor (2017 Student Edition, Autodesk) and fabricated with a 3D printer (Makerbot Replicator 2, U.S.A.). The instrument chassis consists of four items: a bottom enclosure that houses the PCB and the heater, a holder for the blower and for the LED, a casing for the CMOS camera, and an upper enclosure that holds the camera casing and blocks any ambient light from entering the system, see Figures S-3 and S-4. The total printing time for these items, with the printing and travel speed set at 40 mm/s, was ∼20 h. The total weight of these 3D-printed parts is 110 g, equivalent to less than <US$6.

Optical Setup and Analysis. A 23.5 lm LED (475 nm, OSW-6303, Newark) was placed in the holder on the opposite site of the fan, at 10° over the horizontal plane in order to excite solutions inside the chip and to not contaminate the optical path of the CMOS camera. The emitted fluorescence was measured with a Raspberry Camera Module v2 that contains an 8.08MP RGB-CMOS sensor (IMX219, Sony). An optical band-pass filter (520 ± 10 nm, Wratten #58) was placed manually between the CMOS sensor and the lens of the camera module. Detailed information on the optical setup and the development of a graphical user interface (GUI) are provided in the Supporting Information.

Microdevice Fabrication. Devices were designed with CAD software (Inventor, 2017 Student Edition, Autodesk) and fabricated on a 3 mm thick poly(methyl methacrylate) (PMMA) sheet using a high-precision milling machine (MDX-40A, Roland DG, Germany). Further information on the cost and finishing of the microwells can be found in the Supporting Information. The acrylic device sat on top of the resistor surface with a thermistor placed in one of its wells.

Quantitative PCR Assay. Further details on the PCR assay performed in a benchtop thermocycler and our custom-made instrument can be found in the Supporting Information.

RESULTS AND DISCUSSION

3D-Printed Thermal Cycler. Our goal was to develop an intuitive and affordable portable qPCR instrument that could be easily assembled from 3D-printed parts and off-the-shelf components. These characteristics could enable its fast deployment in low-resource settings. Although our instrument is energized with an external power supply, this can be replaced with a portable battery bank with similar power capacity. Other researchers have certainly developed portable and small qPCR

DOI: 10.1021/acs.analchem.7b04843
Anal. Chem. 2018, 90, 5563−5568

instruments; yet to reduce their size, they rely on expensive microfabrication techniques to produce the heating block (e.g., micromachined silicon heaters[3,10,12]) of the thermocycler. In contrast, we leveraged two simple low-cost components, a 5 W ceramic resistor (US$0.45) and a computer fan ($11) to heat and cool a polymeric microdevice. When a voltage is applied across the resistor, the electrical current is converted into heat, reaching temperatures in excess of 100 °C within 1 min. To cool down the resistor and the device, the fan blows room-temperature air. To monitor fluorescence, we utilized a high-power blue LED ($4.3) and a CMOS camera ($26.5) fitted with a plastic band-pass filter to eliminate unwanted fluorescence. The chassis consists of five items fabricated with a 3D printer that are manually assembled; see Figures S-3 and S-4. The total weight of the assembled device is ∼500g, fits in the hand of an adult, and is easily transported. The instrument is controlled with one of the most popular single-board computers, a Raspberry Pi (12.5 millions units sold worldwide to this date). A cross-sectional view of the thermal cycler is shown in Figure 1A, and a photograph of the real instrument is shown in Figure 1B.

Without including the cost of the Raspberry Pi and the touch screen, the cost of our thermocycler ($75 including the power supply) is much cheaper than other low-cost alternatives recently reported that use thermos and a robotic arm to move PCR tubes between water baths held at different temperatures[1,8] or the solar-panel powered PCR.[7] In its current form, the total cost of our thermocycler is $193.2, which is negligible compared to that of a commercial qPCR instrument (> $24 000).[33] An itemized list, including cost of each component can be found in Table S1.

Temperature Control. First, we assessed the capability of the power resistor to reach temperatures in the range of PCR reactions. Although a bare resistor can reach temperatures in excess of 100 °C in less than 1 min, the heat distribution over its surface is not uniform. For example, above 75 °C, there is a difference of at least 25 °C between the resistor ends and its center, Figure 2A. We attribute this difference to the way the resistor is manufactured, with a soldered junction between the resistive element inside the cement and the leads, Figure S-6. This thermal gradient on the surface of the resistor complicates the development of an algorithm to control the temperature and is detrimental to the performance on each reaction in the microwells of the device. To try to homogenize the temperature, we wrapped the resistor's surface with two of the best and economical thermal conductors known: aluminum and copper. Aluminum foil reduced this temperature difference to 4 °C; however, when the resistor is sheathed with copper tape, the temperature difference decreases to less than 0.75 °C, Figure 2B,C. This approach proved to be a simple solution to provide a uniform temperature over the surface of the power resistor.

To control the temperature and program the heating/cooling cycles required for PCR, we developed a proportional-integrative-derivative (PID) controller in Python, a popular open-source software platform. To test our controller, we implemented a real-time PCR (qPCR) protocol that included 2 min at 50 °C for uracyl-N-glycosilase (UNG) incubation, followed by a holding step for 10 min at 95 °C for polymerase activation, completed with 40 PCR cycles at 60 °C for annealing/extending and 90 °C for denaturing. Figure 2D,E shows the temperature traces of this protocol as measured in one of the wells of the device with a thermocouple. We

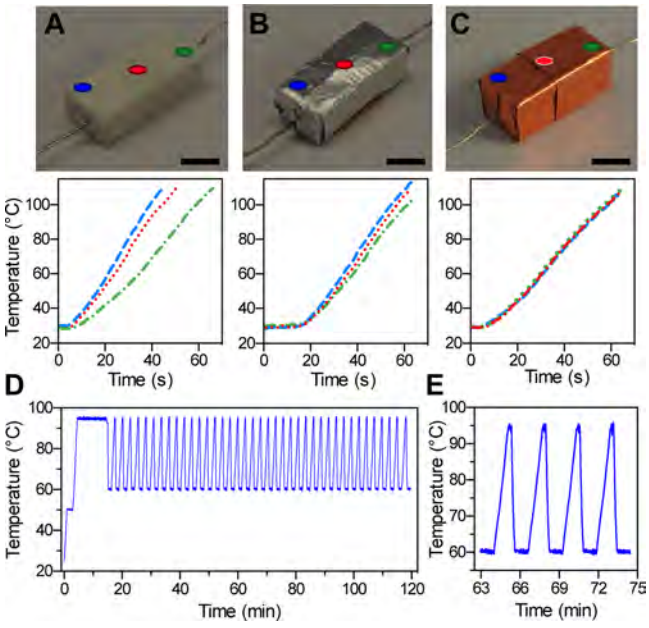

Figure 2. Temperature characterization of the power resistor. Photograph of a bare resistor (A) and a resistor shielded with aluminum foil (B) and copper tape (C). Scale bar, 1 cm. Bottom graphs show traces of the temperature measured on the middle (red dot) and on the edges (blue and green dots) for each power resistor. (D) Representative temperature profile in a microwell for a 40-cycle PCR protocol that starts with 2 min at 50 °C followed by 10 min at 95 °C. (E) Close-up of four PCR cycles.

evaluated the accuracy and precision of the system over the course of these 40 cycles of PCR in our devices. The accuracy was calculated as the difference between the set point and the measured averaged temperature. The precision was defined as the average of the measured standard deviation of the set point temperature. The accuracy of the denaturing step at 95 °C, and the annealing/extension step at 60 °C was 0.15 and 0.18 °C, respectively, while the precision was 0.42 and 0.55 °C. The average heating rate was ∼0.5 °C/s, while the average cooling rate was ∼1.4 °C/s. Our PID controller achieved target temperatures with no observed overshoot. The total time required for a single cycle was ∼150 s and for a 40-cycle PCR was ∼120 min. To achieve faster temperature cycles, the ceramic resistor may be replaced with an array of surface-mount thick-film power resistors.

To assess the performance of our device under different ambient conditions, we evaluated the effect of different ambient temperatures: 20, 30, 35, and 40 °C. The temperature control algorithm performed well on these different conditions, with identical heating and cooling rates (Figure S-7), demonstrating the robustness of our instrument even in harsh climates. Operating under dusty environments may require covering the fan with a filter to deliver clean air into the device.

Compared to other PCR instruments,[10] the thermal cycles produced in our instrument are relative slow, and thus a drawback of our technology, but its high temperature stability and the facility to program the temperature cycles could be easily adapted to perform isothermal NAA assays that are rapidly gaining popularity.[1,2,4,13]

Acrylic Devices and Optical Setup. The acrylic devices feature four 2.1 μL microwells machined on one side on the acrylic. The microwells have a polished round-bottom that helps reduce light artifacts compared to wells with flat bottoms.

DOI: 10.1021/acs.analchem.7b04843
Anal. Chem. 2018, 90, 5563−5568

To facilitate the alignment between the device and the resistor, we engraved a grooved frame on the other side of the device that fits precisely on top of the resistor (Figures 3A,B and S-5.

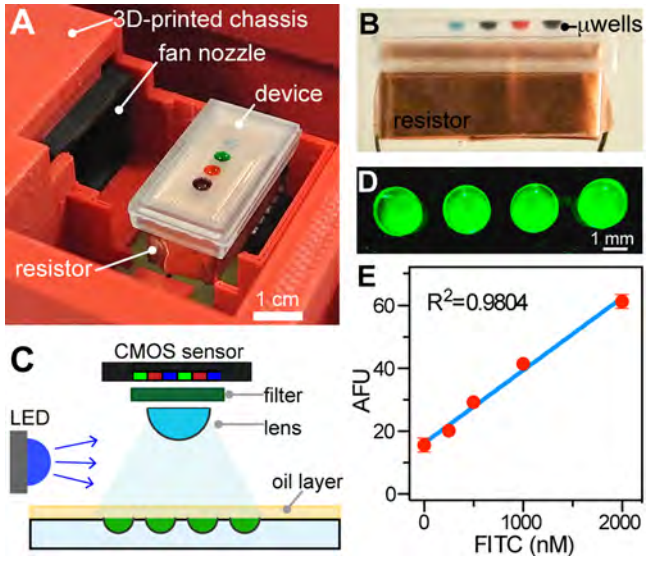

Figure 3. (A) Photograph of a device placed on top of the copper-covered resistor. Note that the fan nozzle points directly to the resistor and the device. (B) Side view of the plastic device over the resistor; micowells are a few mm above the surface. (C) Schematic of the optical setup used to measure fluorescence from each well. (D) Representative fluorescent image captured with the optical setup. Wells were filled with a solution of FITC. (E) Standard curve for a series of dilutions of FITC. Error bars: 1 standard deviation (s.d.), n = 3.

Although these acrylic devices are low-cost, the cost of a milling machine must be factored into their fabrication. Over the past few years, milling machines have become as affordable and user-friendly as 3D printers (see for example the Desktop PCB milling machine, Bantam Tools, U.S.A.).

The instrument was purposely designed to perform real-time PCR on samples that employ TaqMan probes, 6-FAM, a fluorescent intercalating dye (495/520 nm ex/em). As the concentration of DNA amplicons increases exponentially in each cycle, it is accompanied by an increase in fluorescent amplitude. Our optical setup is composed of a high-power blue LED that illuminates the chip from the side, while the camera module that contains a CMOS sensor, is fitted with a band-pass filter and placed a few millimeters above the chip (Figure 3C). The simplicity of our optical setup contrasts other setups that require high expertise to assemble the instrument (e.g., lock-in amplifiers, PMT, and special optical filters and mirrors)[5,12] or that have a repurposed expensive smartphone camera with optic elements to detect and quantify the amplified product.[13,14,16]

Images are acquired using a Python script that (i) controls the camera parameters, (ii) automatically takes images at the end of each PCR cycle, (iii) applies a gamma correction, and (iv) analyzes each microwell of interest. We evaluated the pixel response of the 8-bit digital output sensor as a function of fluorescence intensity (Figure 3D). The camera showed a semilog response for a series of dilutions of FITC, a fluorescent molecule that has an optical spectrum similar to FAM (488/525 nm ex/em), reaching a limit of detection (LOD) of 300 nM (Figure 3E). This scale allowed us to establish an analogous point to measure fluorescence in PCR reactions.

Real-Time PCR. We evaluated the performance of our thermocycler by amplifying the 18S rRNA housekeeping gene at concentrations ranging from 64 pg/μL to 200 ng/μL, spanning 4 orders of magnitude. Using a tablet, we programmed a graphical user interface that displays the temperature and the fluorescence intensity from each well at the end of each PCR cycle (Figure 4A). The change in

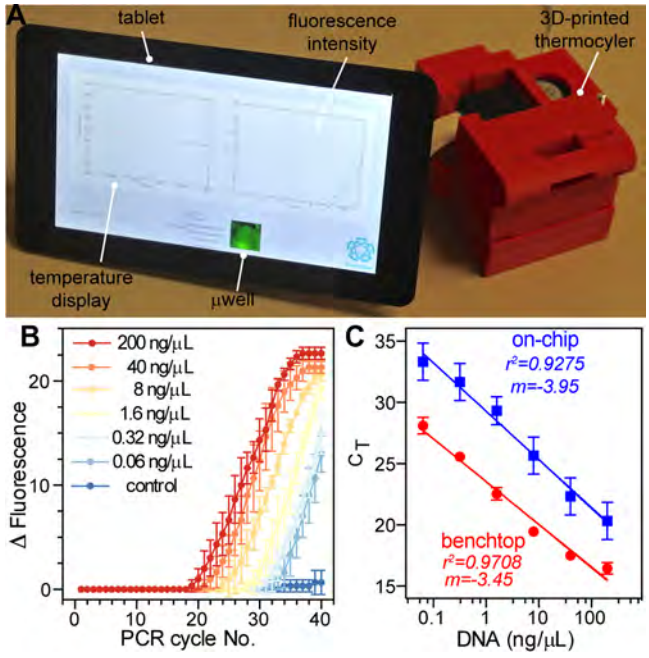

Figure 4. (A) Photograph of the tablet connected to the 3D-printed thermocycler. A graphical user interface displays the temperature and the fluorescence intensity traces of the PCR reactions from each of the four microwells. The Raspberry Pi microcomputer is placed on the back of the tablet. (B) Real-time PCR fluorescence intensity curves plotted against cycle number for six concentrations of DNA and control. Error bars: 1 s.d. for n = 3 performed on different days and on different devices. (C) Comparison of cycle threshold (C_T) values for DNA concentrations spanning 4 orders of magnitude. Blue and red data correspond to our 3D printer and a benchtop thermocycler, respectively.

fluorescence emission intensity at each temperature cycle (ΔF1−F2, where F1 = fluorescence emission at each time point and F2 = fluorescence emission of baseline) was plotted against every cycle number (Figure 4B). Cycle threshold (C_T) values decrease linearly with increasing target concentration. We were able to detect concentrations as low as 64 pg/mL of DNA, while the fluorescent intensity of the negative control (no target) remains nearly zero until the last cycles. This assay was performed on three different days, underscoring the reproducibility of our instrument and of our devices. To test the efficiency of our approach, we compared on-chip vs benchtop qPCR performed under identical experimental conditions (Figure 4C). Both curves had a similar slope, although on-chip reactions in general had higher error bars and lower mean C_T values than benchtop reactions (>4 cycles); however, our thermocycler was able to achieve the same limit of detection (LOD). Additionally, we evaluated the PCR efficiency of each curve, defined by $(10^{-1/k} - 1) \times 100\%$, where k is the slope of the curve as a function of the logarithm of the template

DOI: 10.1021/acs.analchem.7b04843
Anal. Chem. 2018, 90, 5563−5568

concentration. We found that the efficiency for the on-chip based qPCR (79.10%) was considerable lower than for benchtop qPCR (93.11%), an indication of suboptimal reaction conditions. Although we used a hot-start PCR, this limited efficiency for on-chip qPCR in our 3D-printed thermocycler compared to that of the benchtop thermocycler can be attributed to (i) the difference in cycling parameters, (ii) a temperature gradient in the wells, or (iii) to the amount PCR reagents (e.g., nucleotides, enzymes, BSA) used in the reactions. Thus, in its current form, our instrument may not be suitable for applications with low-copy numbers of starting DNA (<100 pg) and for applications that require accurate thermal control, such as sequencing or genotyping experiments, but it may be robust enough for other applications with high-initial DNA quantities such as pathogen detection, differential gene expression, DNA cloning, and colony PCR. However, further optimization of cycling parameters, well size, and amount of PCR reagents, could lead to an improved efficiency and thus increase the portfolio of applications.

CONCLUSIONS

A foremost characteristic of any point-of-care technologies for the developing world is to fulfill the need for low-cost instrumentation that is easy to assemble and fix. This would allow for widespread use of these technologies in low-resource settings and contribute in the diagnosis, treatment, and control of certain diseases. We have demonstrated that a real-time PCR instrument can be made employing off-the-shelf electronics and a CMOS camera, parts that are easy to purchase in most developing countries. The chassis of the instrument is made with a 3D printer, a technology that is becoming ubiquitous thanks to its low cost. 3D printing also enables future improvements to this technology as they become available as well as the ability tailor it to other PCR applications. To control the thermocycler and the optical setup, we utilized a Raspberry Pi and Python, some of the most popular computer and open-source platforms in the world that could expedite the adoption of these technologies in low-resource settings. To make the instrument user-friendly, we used a tablet with a display showing real-time temperature and the change in fluorescence intensity inside the wells of the device as the PCR reaction unfolds.

The instrument allowed us to perform PCR on a series of dilutions of DNA and obtain quantitative measurements of the initial amount of genetic material in the samples. Although our instrument did not perform as well as a commercial thermocycler, as measured by the C_T efficiency, several parameters such as the size of the microwells and the amount of reagents used in each PCR reaction could be optimized to improve the efficiency. Notably, our instrument can be readily utilized in isothermal NAA assays.

ASSOCIATED CONTENT

Supporting Information

The Supporting Information is available free of charge on the ACS Publications website at DOI: 10.1021/acs.analchem.7b04843.

Detailed fabrication on the optical setup, the microwells, and the PCRS assay. Schematics of the electronic designs; photographs of the individual 3D-printed parts, the device, and the power resistor; traces of PCR cycles at different external temperature conditions (PDF)

AUTHOR INFORMATION

Corresponding Author

*E-mail: jlgarciac@cinvestav.mx.

ORCID

Jose L. Garcia-Cordero: 0000-0002-3868-7405

Author Contributions

The manuscript was written through contributions of all authors. All authors have given approval to the final version of the manuscript.

Notes

The authors declare no competing financial interest.

ACKNOWLEDGMENTS

This work was funded by Mexico's CONACyT under grants No. 256097, 262771, and FC-1132. We would like to thank Prof. Chris Backhouse & Samuel Tristan for helpful discussions.

REFERENCES

(1) Chan, K.; Weaver, S. C.; Wong, P. Y.; Lie, S.; Wang, E.; Guerbois, M.; Vayugundla, S. P.; Wong, S. *Sci. Rep.* **2016**, *6*, 38223.

(2) Liao, S. C.; Peng, J.; Mauk, M. G.; Awasthi, S.; Song, J. Z.; Friedman, H.; Bau, H. H.; Liu, C. C. *Sens. Actuators, B* **2016**, *229*, 232−238.

(3) Ahrberg, C. D.; Manz, A.; Neuzil, P. *Anal. Chem.* **2016**, *88*, 4803−4807.

(4) Song, J. Z.; Mauk, M. G.; Hackett, B. A.; Cherry, S.; Bau, H. H.; Liu, C. C. *Anal. Chem.* **2016**, *88*, 7289−7294.

(5) Xu, G. L.; Hsieh, T. M.; Lee, D. Y. S.; Ali, E. M.; Xie, H.; Looi, X. L.; Koay, E. S. C.; Li, M. H.; Ying, J. Y. *Lab Chip* **2010**, *10*, 3103−3111.

(6) Lafleur, L. K.; Bishop, J. D.; Heiniger, E. K.; Gallagher, R. P.; Wheeler, M. D.; Kauffman, P.; Zhang, X. H.; Kline, E. C.; Buser, J. R.; Kumar, S.; Byrnes, S. A.; Vermeulen, N. M. J.; Scarr, N. K.; Belousov, Y.; Mahoney, W.; Toley, B. J.; Ladd, P. D.; Lutz, B. R.; Yager, P. *Lab Chip* **2016**, *16*, 3777−3787.

(7) Jiang, L.; Mancuso, M.; Lu, Z. D.; Akar, G.; Cesarman, E.; Erickson, D. *Sci. Rep.* **2015**, *4*, 4137.

(8) Wong, G.; Wong, I.; Chan, K.; Hsieh, Y. C.; Wong, S. *PLoS One* **2015**, *10* (7), e0131701.

(9) Chan, K. F.; Wong, P. Y.; Yu, P.; Hardick, J.; Wong, K. Y.; Wilson, S. A.; Wu, T.; Hui, Z.; Gaydos, C.; Wong, S. S. *PLoS One* **2016**, *11* (2), e0149150.

(10) Ahrberg, C. D.; Ilic, B. R.; Manz, A.; Neuzil, P. *Lab Chip* **2016**, *16*, 586−592.

(11) Lounsbury, J. A.; Karlsson, A.; Miranian, D. C.; Cronk, S. M.; Nelson, D. A.; Li, J. Y.; Haverstick, D. M.; Kinnon, P.; Saul, D. J.; Landers, J. P. *Lab Chip* **2013**, *13*, 1384−1393.

(12) Neuzil, P.; Novak, L.; Pipper, J.; Lee, S.; Ng, L. F. P.; Zhang, C. Y. *Lab Chip* **2010**, *10*, 2632−2634.

(13) Priye, A.; Bird, S. W.; Light, Y. K.; Ball, C. S.; Negrete, O. A.; Meagher, R. J. *Sci. Rep.* **2017**, *7*, 44778.

(14) Walker, F. M.; Ahmad, K. M.; Eisenstein, M.; Soh, H. T. *Anal. Chem.* **2014**, *86*, 9236−9241.

(15) Niemz, A.; Ferguson, T. M.; Boyle, D. S. *Trends Biotechnol.* **2011**, *29*, 240−250.

(16) Priye, A.; Wong, S. S.; Bi, Y. P.; Carpio, M.; Chang, J.; Coen, M.; Cope, D.; Harris, J.; Johnson, J.; Keller, A.; Lim, R.; Lu, S.; Millard, A.; Pangelinan, A.; Patel, N.; Smith, L.; Chan, K. F.; Ugaz, V. M. *Anal. Chem.* **2016**, *88*, 4651−4660.

(17) Bennett, D. E.; Bertagnolio, S.; Sutherland, D.; Gilks, C. F. *Antivir Ther* **2008**, *13*, 1−13.

(18) Angione, S. L.; Chauhan, A.; Tripathi, A. *Anal. Chem.* **2012**, *84*, 2654−2661.

(19) Lagally, E. T.; Scherer, J. R.; Blazej, R. G.; Toriello, N. M.; Diep, B. A.; Ramchandani, M.; Sensabaugh, G. F.; Riley, L. W.; Mathies, R. A. *Anal. Chem.* **2004**, *76*, 3162−3170.

DOI: 10.1021/acs.analchem.7b04843
Anal. Chem. 2018, 90, 5563−5568

(20) Liu, P.; Seo, T. S.; Beyor, N.; Shin, K. J.; Scherer, J. R.; Mathies, R. A. *Anal. Chem.* **2007**, *79*, 1881−1889.
(21) Kaigala, G. V.; Hoang, V. N.; Stickel, A.; Lauzon, J.; Manage, D.; Pilarski, L. M.; Backhouse, C. J. *Analyst* **2008**, *133*, 331−338.
(22) Wheeler, E. K.; Benett, W.; Stratton, P.; Richards, J.; Chen, A.; Christian, A.; Ness, K. D.; Ortega, J.; Li, L. G.; Weisgraber, T. H.; Goodson, K.; Milanovich, F. *Anal. Chem.* **2004**, *76*, 4011−4016.
(23) Agrawal, N.; Hassan, Y. A.; Ugaz, V. M. *Angew. Chem., Int. Ed.* **2007**, *46*, 4316−4319.
(24) Xiang, Q.; Xu, B.; Li, D. *Biomed. Microdevices* **2007**, *9*, 443−449.
(25) Chung, K. H.; Park, S. H.; Choi, Y. H. *Lab Chip* **2010**, *10*, 202−210.
(26) Hsieh, Y. F.; Lee, D. S.; Chen, P. H.; Liao, S. K.; Yeh, S. H.; Chen, P. J.; Yang, A. S. *Sens. Actuators, B* **2013**, *183*, 434−440.
(27) Tsai, Y. L.; Wang, H. T.; Chang, H. F.; Tsai, C. F.; Lin, C. K.; Teng, P. H.; Su, C.; Jeng, C. C.; Lee, P. Y. *PLoS One* **2012**, *7*, e45278.
(28) Lim, S.; Nan, H.; Lee, M. J.; Kang, S. H. *J. Chromatogr. B: Anal. Technol. Biomed. Life Sci.* **2014**, *963*, 134−139.
(29) Tanriverdi, S.; Chen, L.; Chen, S. *J. Infect. Dis.* **2010**, *201* (Suppl 1), S52−S58.
(30) Shu, B.; Zhang, C.; Xing, D. *Biosens. Bioelectron.* **2017**, *97*, 360−368.
(31) Pak, N.; Saunders, D. C.; Phaneuf, C. R.; Forest, C. R. *Biomed. Microdevices* **2012**, *14*, 427−433.
(32) Qiu, X.; Mauk, M. G.; Chen, D.; Liu, C.; Bau, H. H. *Lab Chip* **2010**, *10*, 3170−3177.
(33) Mothershed, E. A.; Whitney, A. M. *Clin. Chim. Acta* **2006**, *363*, 206−220.

DOI: 10.1021/acs.analchem.7b04843
Anal. Chem. 2018, 90, 5563−5568